

## Tribological properties of nanostructured $\text{Al}_2\text{O}_3$ –40% $\text{TiO}_2$ multiphase ceramic particles reinforced Ni-based alloy composite coatings

Long HE, Ye-fa TAN, Hua TAN, Chun-hua ZHOU, Li GAO

Engineering Institute of Engineering Corps, PLA University of Science and Technology, Nanjing 210007, China

Received 10 July 2012; accepted 20 December 2012

**Abstract:** The Ni-based alloy composite coatings reinforced by nanostructured  $\text{Al}_2\text{O}_3$ –40% $\text{TiO}_2$  multiphase ceramic particles were prepared on the surface of 7005 aluminum alloy by plasma spray technology. The microstructure and tribological properties of the composite coatings were researched. The results show that the composite coatings mainly consist of  $\gamma$ -Ni,  $\alpha$ - $\text{Al}_2\text{O}_3$ ,  $\gamma$ - $\text{Al}_2\text{O}_3$  and rutile- $\text{TiO}_2$  etc, and exhibit lower friction coefficients and wear losses than the Ni-based alloy coatings at different loads and speeds. The composite coating bears low contact stress at 3 N and its wear mechanism is micro-cutting wear. As loads increase to 6–12 N, the contact stress is higher than the elastic limit stress of worn surface, and the wear mechanisms change into multi-plastic deformation wear, micro-brittle fracture wear and abrasive wear. With the increase of speeds, the contact temperature of worn surface increases. The composite coating experiences multi-plastic deformation wear, fatigue wear and adhesive wear.

**Key words:** nanostructured  $\text{Al}_2\text{O}_3$ – $\text{TiO}_2$  multiphase ceramic particles; Ni-based alloy; composite coating; plasma spray; friction; wear

### 1 Introduction

Aluminum alloys have become the important materials to achieve lightweight of machinery due to their low density, high specific strength, good electrical and thermal conductivity, which are widely used in mechanical industry, aerospace industry, national defense and other high-tech areas [1,2]. However, it is hard for aluminum alloy frictional parts to meet the needs of severely abrasive working condition because of the low hardness and poor wear resistance that restrain their further applications to a great extent [3,4].

Plasma spray technology possesses convenient process, high efficiency and excellent coating performance, which shows great effect and application potential in surface repairing and strengthening of mechanical parts made of light metals [5–7]. For example, ALTUNPAK et al [8] prepared SiC particles reinforced Al–Si composite coating on the surface of aluminum alloy by plasma spray. The generation of  $\text{Al}_4\text{C}_3$  brittle phase by reactions between particle and matrix in foundry or sintering process was avoided and the composite coating exhibited better wear resistance

than the substrate. The plasma spraying  $\text{Al}_2\text{O}_3$ /Ni–Cr– $\text{Cr}_3\text{C}_2$  composite coatings prepared by CHEN et al [9] showed a low friction coefficient of 0.0179 and wear ratio of  $6.7 \times 10^{-4}$  compared with the 7A55 aluminum alloy substrate. With the development of nanotechnology, nanostructured  $\text{Al}_2\text{O}_3$ – $\text{TiO}_2$  series multi-phase ceramic particles are widely used in plasma spray, the coatings prepared own excellent friction and wear properties. RICO et al [10] studied the tribological properties of plasma spraying  $\text{Al}_2\text{O}_3$ –13% $\text{TiO}_2$  nano and micron coatings, and found that the friction coefficient of nano coating was lower than that of the micron coating and the wear loss was reduced by 1.5 times. LU et al [11] also discovered that the friction coefficient and wear loss of  $\text{Al}_2\text{O}_3$ –13% $\text{TiO}_2$  nano coating were low compared with the micron coating, indicating good anti-friction and anti-wear properties.

Owing to the excellent anti-wear, anti-corrosion and anti-high temperature oxidation properties [12], plasma spraying Ni-based alloy coatings are capable of improving the wear resistance of aluminum alloy frictional parts as surface strengthening coatings. Nevertheless, the increasingly severe working conditions call for better tribological properties of Ni-based alloy

coatings. Therefore, it is an urgent problem to further improve their wear resistance in order to prolong the service lives of aluminum alloy frictional parts. In this work, nanostructured  $\text{Al}_2\text{O}_3$ -40% $\text{TiO}_2$  multi-phase ceramic particles reinforced Ni-based alloy (n-AT40/Ni-based alloy) composite coatings were prepared on the surface of 7005 aluminum alloy using plasma spray technology. The tribological behavior and wear mechanisms of the composite coatings were investigated to provide theoretical basis and experimental data for further augment in wear resistance of Ni-based alloy coatings.

## 2 Experimental

### 2.1 Specimen preparation

The spraying composite materials were composed of Ni-based alloy powders and n-AT40 agglomerated particles with volume ratio of 3:2. The chemical composition of the Ni-based alloy powders with size ranging from 55  $\mu\text{m}$  to 128  $\mu\text{m}$  was 15.5% Cr, 3.5% B, 4.0% Si, 15.0% Fe, 3.0% W, 0.8% C and residue of Ni (in mass fraction). The reinforcing n-AT40 particles with sizes from 20  $\mu\text{m}$  to 60  $\mu\text{m}$  were agglomerated of 60%  $\text{Al}_2\text{O}_3$  and 40%  $\text{TiO}_2$  nanoparticles whose original sizes were from 30 nm to 80 nm. The morphologies of the n-AT40 agglomerated particle and the spraying composite powders are shown in Fig. 1.

7005 aluminum alloy was chosen as substrate and its chemical composition was 4.0%–5.0% Zn, 1.0%–1.8% Mg, 0.2%–0.7% Mn, 0.4% Fe, 0.35% Si, 0.1% Cu and residue of Al. Prior to spraying, the substrates were treated by sanding, ultrasonic cleaning and sandblasting. The n-AT40/Ni-based alloy composite coatings were prepared on the surface of substrate with the thickness of 200  $\mu\text{m}$  by a DH-1080 plasma spray equipment. The technical parameters were electric current of 500 A, voltage of 50 V and spray distance of 100 mm. The Ni-based alloy coatings were also prepared as comparison. The sprayed samples were ground by diamond wheel and diamond abrasive paste of W0.5 to the surface roughness of 0.5  $\mu\text{m}$ , and incised into test pieces with the dimensions of 12 mm $\times$ 12 mm $\times$ 6 mm by wire-electrode cutting.

### 2.2 Tribological tests

Tribological tests were carried out in an HT-500 ball-on-disc tribometer at room temperature of 25  $^\circ\text{C}$ . The upper specimen was a GCr15 ball with diameter of 4 mm and microhardness of  $\text{HV}_{0.5}$  800. The down one was the composite coating or the Ni-based alloy coating test piece. The GCr15 ball slid against the coatings under dry friction at the loads of 3, 6, 9 and 12 N and the

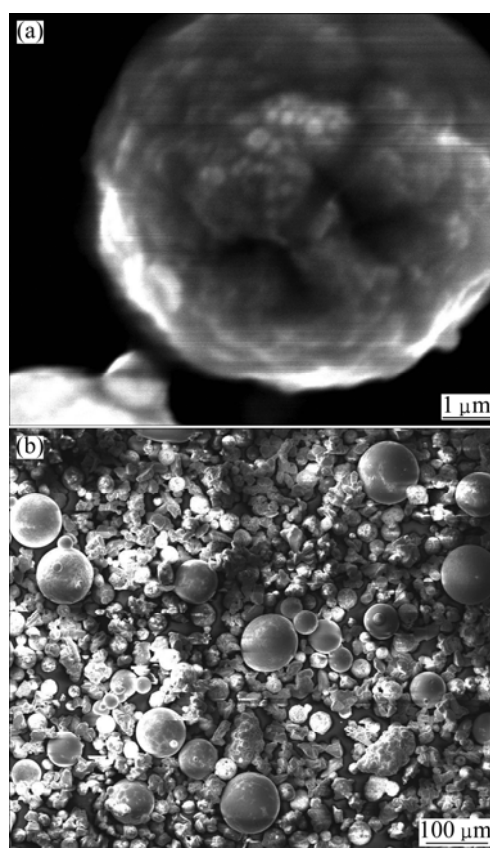


**Fig. 1** Morphologies of n-AT40 agglomerated particle (a) and spraying composite powders (b)

speeds of 0.21, 0.28, 0.35 and 0.42 m/s for a distance of 500 m. Friction coefficients were tested by the software attached to HT-500. Wear losses were measured using a TG328B balance with precision of 0.1 mg.

### 2.3 Surface analysis

A FEIQUANTA200 scanning electron microscope (SEM) with energy-dispersive X-ray spectroscope (EDX) was employed to observe the microstructure and worn surfaces morphologies of the coatings, and test the elemental composition. The phase composition of the coatings was tested by a D-MAX/R X-ray diffractometer (XRD). The microhardness of the coatings was measured by a DHV-1000 microhardness tester. The bonding strength between the composite coating and the substrate was obtained by a CMT(5105) electronic universal testing machine according to the national standard of GB/T 8642—1988.

## 3 Results and discussion

### 3.1 Microstructure

The morphologies and EDX spectra of n-AT40/Ni-based alloy composite coatings are shown in Fig. 2. It shows that the composite coating takes on typical

lamellar structure. A few pores, microcracks and some unmelted particles with submicron structure are observed in Figs. 2(a) and (b). The composite coating integrates tightly with the aluminum alloy substrate and the bonding strength between them is 32.8 MPa. According to the EDX spectra of the light area marked by *A* (Fig. 2(c)) and the dark lamella area marked by *B* (Fig. 2(d)), the main elements in area *A* are Ni, Cr, Fe and Si, so it is the Ni-based alloy matrix. Area *B* where is enriched with elements of Al, Ti and O is the n-AT40 reinforcing phase. In plasma spraying process, the molten particles impinging onto the substrate surface at high speed are deformed, spread and deposited to form

the typical lamellar structure. The residual air in the composite coating and the non-integrated deposition among lamellas leads to pores. Besides, because of the differences in super cooling and solidification rate, the deformation extent of spraying particles is different, which results in residual tensile stress and induces microcracks. The submicron structure in the composite coating is attributed to partial sintering and growing up of a few incompletely molten n-AT40 particles [13].

Figure 3 shows the XRD patterns of the Ni-based alloy coating and the composite coating. It can be seen that the phase composition of Ni-based alloy coating is  $\gamma$ -Ni, CrB,  $\text{Cr}_7\text{C}_3$ ,  $\text{Cr}_{23}\text{C}_6$  and  $\text{FeNi}_3$  (Fig. 3(a)), moreover,

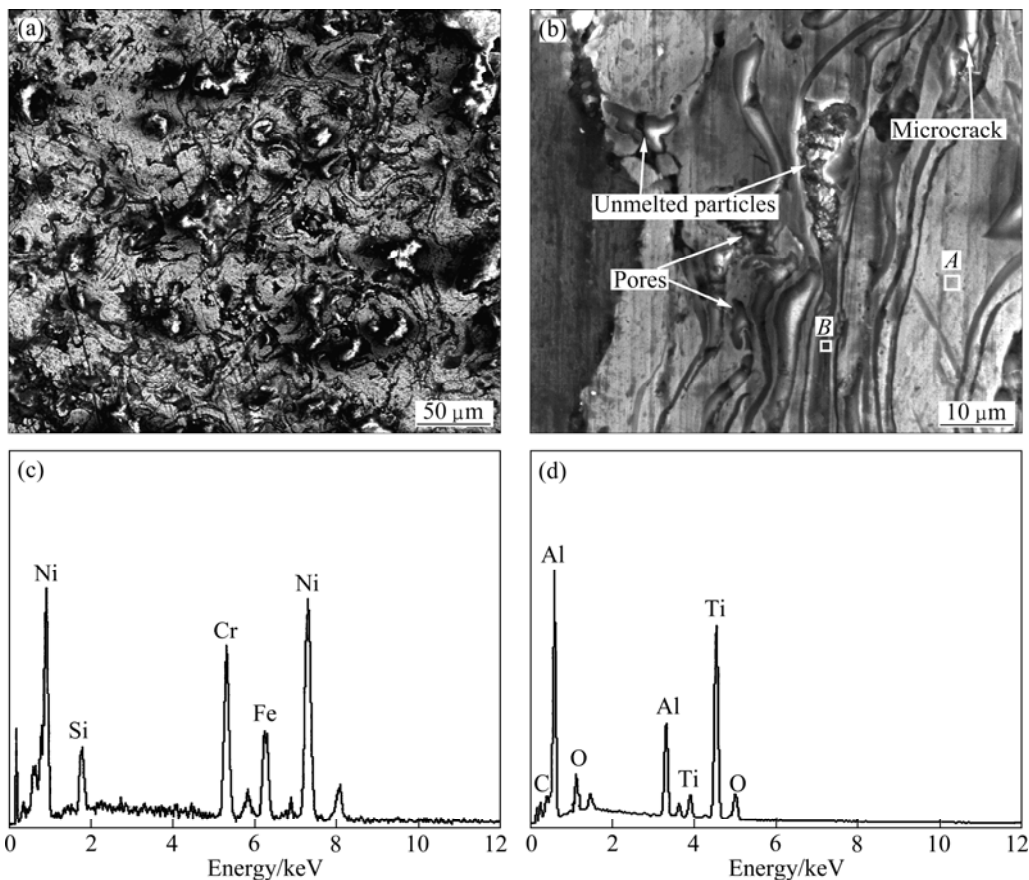


Fig. 2 SEM images of surface (a), cross-section (b) and EDX spectra of area *A* (c) and area *B* (d) of composite coatings

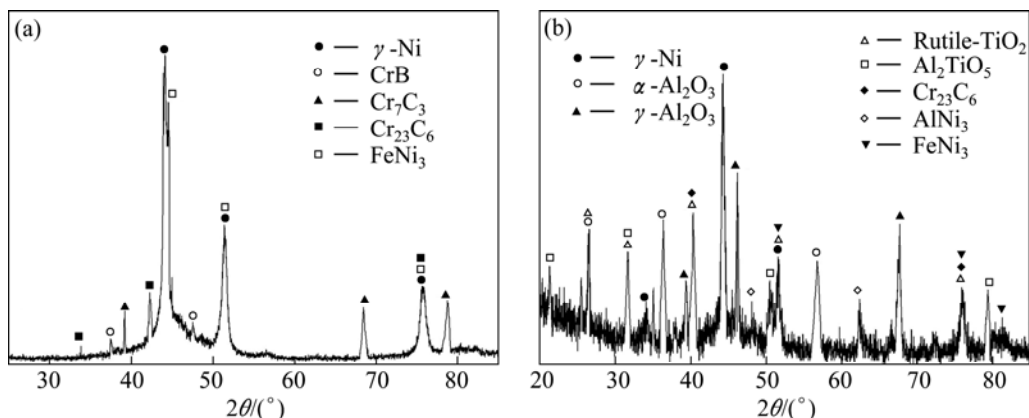


Fig. 3 XRD patterns of Ni-based alloy coating (a) and composite coating (b)

the reinforcing phases of  $\alpha$ -Al<sub>2</sub>O<sub>3</sub>,  $\gamma$ -Al<sub>2</sub>O<sub>3</sub>, rutile-TiO<sub>2</sub>, Al<sub>2</sub>TiO<sub>5</sub> and AlNi<sub>3</sub> are also included in the composite coating according to Fig. 3(b). Due to the heating effect of plasma arc, the temperature of reinforcing particles increases fast. When the temperature is higher than 630 °C, anatase-TiO<sub>2</sub> phase in reinforcing particles experiences phase transformation and turns into rutile-TiO<sub>2</sub> phase [14]. At the temperature ranging from 1850 °C (melting point of TiO<sub>2</sub>) to 2050 °C (melting point of Al<sub>2</sub>O<sub>3</sub>), element diffusion among the solid  $\alpha$ -Al<sub>2</sub>O<sub>3</sub> and the molten rutile-TiO<sub>2</sub> and  $\gamma$ -Ni occurs to decrease the interface energy gradient and increase the bonding strength among nanoparticles. When the temperature is higher than 2050 °C, Al<sub>2</sub>O<sub>3</sub>, TiO<sub>2</sub> and  $\gamma$ -Ni are all in molten state, which leads to the formation of Al<sub>2</sub>TiO<sub>5</sub> and AlNi<sub>3</sub> phases as a result of chemical reactions. In addition, solidification rate of the molten particles is so fast that non-equilibrium crystallization of partial  $\alpha$ -Al<sub>2</sub>O<sub>3</sub> phase occurs to generate the unstable  $\gamma$ -Al<sub>2</sub>O<sub>3</sub> phase, which forms the coexistence structure of  $\alpha$ -Al<sub>2</sub>O<sub>3</sub> and  $\gamma$ -Al<sub>2</sub>O<sub>3</sub> in the composite coating.

The grain size of  $\alpha$ -Al<sub>2</sub>O<sub>3</sub> and  $\gamma$ -Al<sub>2</sub>O<sub>3</sub> can be calculated by the Scherrer formula as [15]

$$d_c = \frac{K\lambda}{\beta \cos \theta} \quad (1)$$

where  $d_c$  is the grain size,  $K$  is constant,  $\lambda$  is the wavelength of X-ray,  $\beta$  is the full width at half maximum, and  $\theta$  is the diffraction angle.

The average grain sizes of  $\alpha$ -Al<sub>2</sub>O<sub>3</sub> and  $\gamma$ -Al<sub>2</sub>O<sub>3</sub> phases are respectively 39.45 nm and 33.57 nm, indicating the existence of nanostructure in the composite coating as shown in Fig. 4, which is beneficial to improve the microstructure and tribological properties of the composite coating.

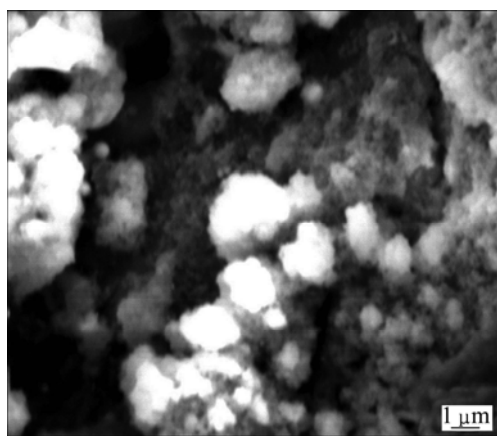


Fig. 4 SEM image showing nanostructure in composite coating

### 3.2 Microhardness

The cross-section microhardness of the composite coating is shown in Fig. 5. It is found that the

microhardness of the composite coating is HV<sub>0.5</sub>624, which is 13.5% higher than that of the Ni-based alloy coating, but takes on a decreasing trend with the increase of distance to surface. Because of the uniformly distributed n-AT40 hard particles, dislocation of the  $\gamma$ -Ni solid solution in plastic deformation process is blocked to strengthen its deformation resistance [16]. Besides, some nanoparticles precipitated at grain boundaries are able to enhance the nucleation rate and restrain the growth of coating grains. According to the Hall-Petch equation [17]:

$$\sigma_V = \sigma_0 + k \cdot d^{-0.5} \quad (2)$$

where  $\sigma_V$  is the yield strength of Ni-based alloy matrix,  $\sigma_0$  and  $k$  are constants, and  $d$  is the average grain size.

The yield strength of Ni-based alloy matrix increases rapidly with the decrease of average grain size, so the plastic deformation resistance of the composite coating is further enhanced, which results in higher microhardness than the Ni-based alloy coating.

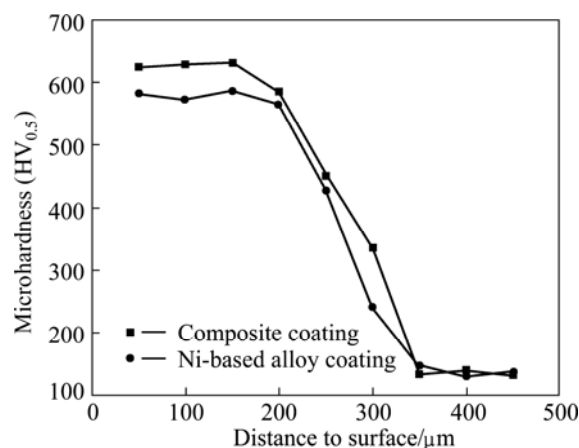


Fig. 5 Microhardness distribution of composite coating on cross section

### 3.3 Tribological behavior and wear mechanisms

#### 3.3.1 Effects of loads on friction and wear properties of composite coatings

The friction and wear results of the n-AT40/Ni-based alloy composite coatings at different loads are shown in Fig. 6. It can be seen that the friction coefficients of the composite coatings increase from 0.360 to 0.394 with the increase of loads, which are lower than those of the Ni-based alloy coatings ranging from 0.383 to 0.438 (Fig. 6(a)). At the load of 3 N, the composite coating is in a slight wear condition and its wear loss is 1.32 mg. When the loads are in the range of 6–9 N, the composite coating is in the moderate wear stage, in which the wear losses increase to the range of 2.60–2.85 mg. At the heavy load of 12 N, the composite coating suffers from severe wear with the wear loss of

4.49 mg, but which is still lower than that of the Ni-based alloy coating (Fig. 6(b)). On one hand, due to the grain refinement effect caused by n-AT40 particles, the strength and deformation resistance of the composite coating are increased, which results in the improvement on its tribological properties. On the other hand, the reinforcing particles are capable of restraining crack propagation and alleviating fatigue fracture, so the wear resistance of the composite coating is further improved.

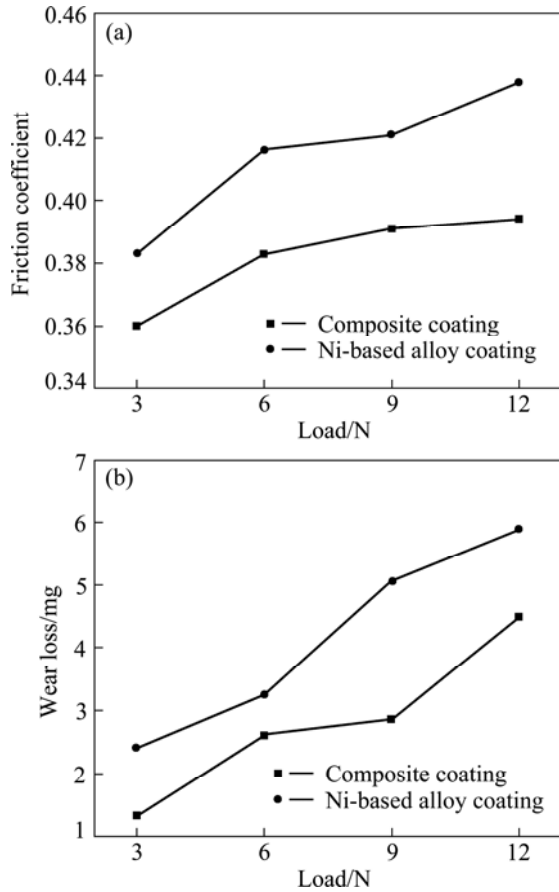


**Fig. 6** Friction coefficient (a) and wear loss (b) of composite coatings at different loads

Loads affect the tribological properties of the composite coating by changing its stress state on the worn surface. Taking frictional contact between the composite coating and the GCr15 counterpart into consideration, the elastic limit stress of worn surface of the composite coating  $(p_0)_y$  based on the Mises rule can be expressed as [18]

$$(p_0)_y = \sigma_c / \left[ \frac{(1-2\nu_1)^2}{3} + \frac{(1-2\nu_1)(2-\nu_1)\mu_F\pi}{4} + \frac{(16-4\nu_1+7\nu_1^2)\mu_F^2\pi^2}{64} \right]^{1/2} \quad (3)$$

where  $\nu_1$  is the Poisson ratio of the composite coating,  $\mu_F$  is the friction coefficient at different loads, and  $\sigma_c$  is the

yield strength of the composite coating.

Moreover, the relationship between the yield strength ( $\sigma_c$ ) and the indentation hardness ( $\sigma_b$ ) of the composite coating is as follows:

$$\sigma_c \approx \frac{1}{2.8} \sigma_b = \frac{1}{2.8} \frac{F}{A} \quad (4)$$

where  $F$  is the load applied to the indenter, and  $A$  is the indentation area.

Load ( $F$ ) can be expressed by the Vicker's microhardness ( $H_V$ ), i.e.

$$F = \frac{H_V g}{1.854} d_1^2 \quad (5)$$

where  $H_V$  is the Vicker's microhardness of the composite coating,  $d_1$  is the cater-corner length of indentation, and  $g$  is the acceleration of gravity.

The relationship between the indentation cater-corner length ( $d_1$ ) and the indentation area ( $A$ ) is as follows:

$$A = \frac{d_1^2}{2} \left( \sin\left(\frac{\alpha}{2}\right) \right)^{-1} \quad (6)$$

where  $\alpha$  is the angle of the taper indenter of  $136^\circ$ .

Substituting Eqs. (5) and (6) into Eq. (4), the yield strength ( $\sigma_c$ ) of the composite coating can be obtained:

$$\sigma_c = \frac{1}{2.8 \times 1.854} H_V 2g \sin\left(\frac{\alpha}{2}\right) \quad (7)$$

Therefore, the elastic limit stress of the composite coating can be calculated by the following equation:

$$(p_0)_y = \left[ \frac{1}{2.8 \times 1.854} H_V 2g \sin\left(\frac{\alpha}{2}\right) \right] / \left[ \frac{(1-2\nu_1)^2}{3} + \frac{(1-2\nu_1)(2-\nu_1)\mu_F\pi}{4} + \frac{(16-4\nu_1+7\nu_1^2)\mu_F^2\pi^2}{64} \right]^{1/2} \quad (8)$$

The elastic limit stress of the composite coating characterizes its maximum permissible contact stress when plastic deformation happens. If the contact stress is higher than the elastic limit stress, yield flow and plastic deformation of the composite coating will be generated. Some researches [19] have proved that friction force hardly affects normal stress, which can be ignored. In order to research the effects of loads on tribological properties of the composite coatings, the Hertz formula of rigid sphere and elastic half-plane contact under normal loads can be used to calculate the contact stress of worn surface [20]:

$$p_0 = \left[ \frac{6P}{\pi^3 R^2} \left( \frac{E_1}{1-\nu_1^2} \right)^2 \right]^{1/3} \quad (9)$$

where  $P$  is the load applied to the GCr15 steel ball;  $E_1$  is the elastic modulus of the composite coating;  $R$  is the comprehensive curvature radius, i.e.

$$\frac{1}{R} = \frac{1}{R_1} + \frac{1}{R_2}$$

$R_1$  and  $R_2$  are curvature radius of the frictional pairs.

The surface contact stress ( $p_0$ ) and elastic limit stress ( $(p_0)_y$ ) of the composite coating at different loads are listed in Table 1.

The typical worn surface morphologies of n-AT40/Ni-based alloy composite coatings at different loads and the EDX spectra of worn surface at 12 N are shown in Fig. 7. It is found that there are only some shallow scratches on the worn surface at 3 N (Fig. 7(a)). In this friction condition, the surface contact stress of the

**Table 1** Surface contact stress and elastic limit stress of composite coatings at different loads

Load/N	Elastic limit stress/MPa	Contact stress/MPa
3	2811.62	2267.23
6	2691.68	2856.54
9	2652.26	3269.92
12	2637.76	3599.02

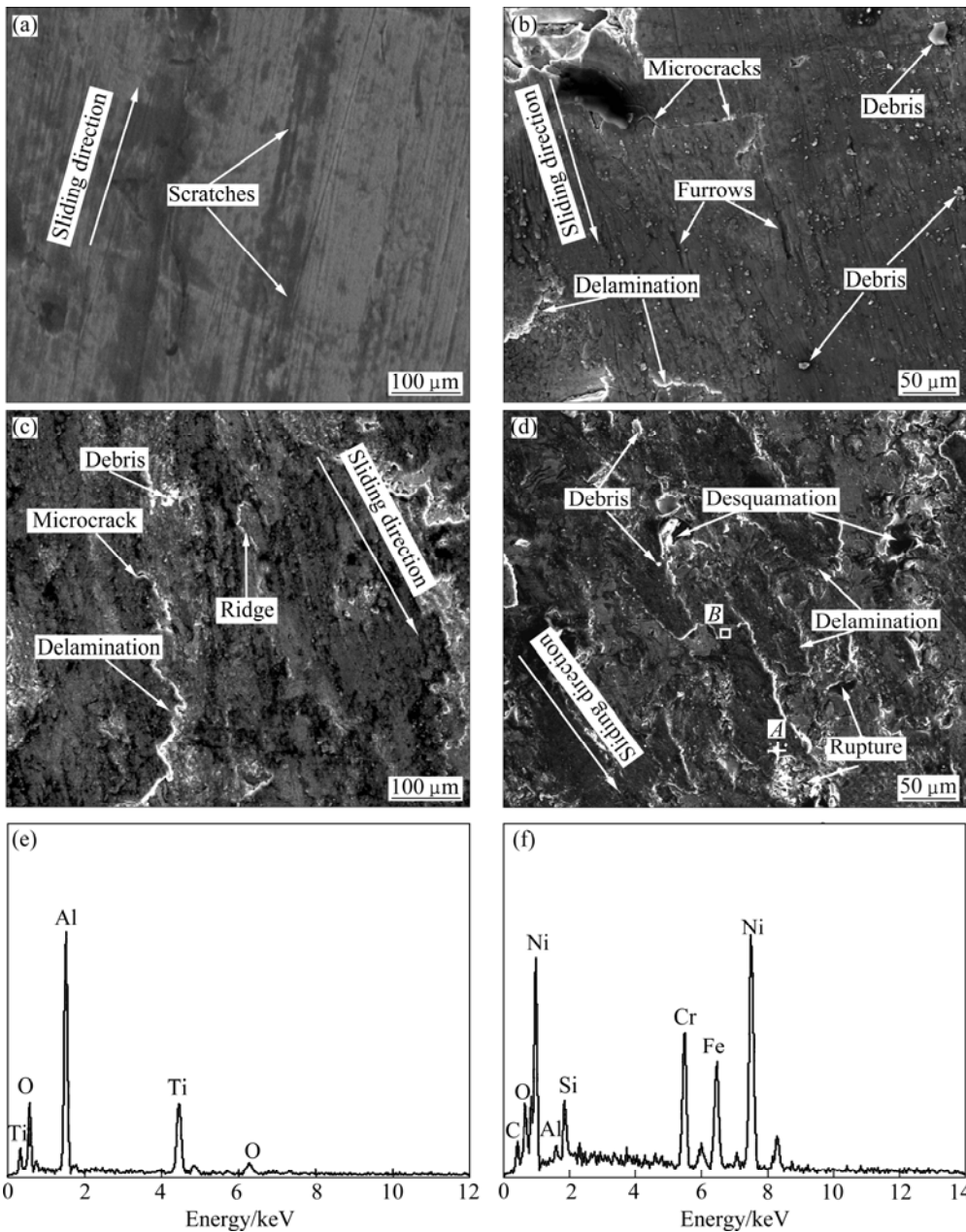


**Fig. 7** Typical worn surface morphologies of composite coatings at 3 N (a), 6 N (b), 9 N (c), 12 N (d) and EDX spectra of area A (e) and area B (f) on worn surface at 12 N in Fig. 7(d)

composite coating is 2267.23 MPa, which is smaller than its elastic limit stress of 2811.62 MPa, no obvious plastic deformation of the composite coating occurs and its wear mechanism is mainly micro-cutting wear caused by the GCr15 counterpart, so the composite coating is in a slight wear condition.

As loads increase to the range of 6–9 N, there are delamination, furrows and ridges as well as microcracks on the worn surfaces as shown in Figs. 7(b) and (c), which indicates that the composite coating suffers from multi-plastic deformation wear and abrasive wear. The schematic wear mechanisms are depicted in Fig. 8. At the load of 6 N, the surface contact stress of the composite coating is 2856.54 MPa, which is 6.1% higher than its elastic limit stress, and increases to 3269.92 MPa at 9 N. Under the ploughing and extruding of GCr15 counterpart, the composite coating experiences yield flow and plastic deformation, leading to delamination and ridge. Additionally, the deformed layer is desquamated by repeating friction, and then is extruded into small debris acting as abrasive, resulting in furrows and edges. Therefore, the wear loss of the composite coating at 9 N is much higher than that at 3 N. Owing to the strengthening effect caused by n-AT40 particles, surface hardness and deformation resistance of the composite coating are enhanced, so the composite coating shows better tribological properties than the Ni-based alloy coating.

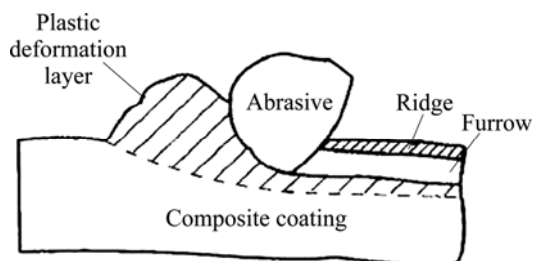


**Fig. 8** Schematic diagram of multi-plastic deformation wear and abrasive wear

With loads increasing to 12 N, the worn surface of the composite coating becomes much rougher, where exist discontinuous deformed layer, local brittle desquamation and some wear debris as shown in Fig. 7(d). According to the EDX spectra of the debris marked by *A* (Fig. 7(e)) and the deformed layer marked by *B* (Fig. 7(f)), the elemental composition of debris is Al, Ti and O, indicating that it is the desquamated n-AT40 reinforcing phase. The deformed layer which mainly consists of Ni, Fe, Cr and Si is the Ni-based alloy matrix. At the heavy load of 12 N, the surface contact stress of the composite coating is 3599.02 MPa, which results in much more severe plastic deformation. Work hardening of the worn surface happens because of

repeating extruding and cutting by GCr15 counterpart, which increases the brittleness of the composite coating. As a result, the formation, propagation and intersection of microcracks on the worn surface are accelerated to induce micro-brittle fracture wear. Furthermore, a few n-AT40 particles with low bonding strength to  $\gamma$ -Ni base phase are worn off in plastic deformation process, leading to abrasive wear. However, most of the uniformly distributed n-AT40 particles in the composite coating are able to produce nail-blocking effect on microcracks and decrease crack tip energy, which is helpful to alleviating the brittle fracture wear of the composite coating [21–23]. Therefore, there is little desquamation of the composite coating occurring in the heavy load friction condition [24], and the wear loss of the composite coating is small compared with the Ni-based alloy coating.

### 3.3.2 Effects of speeds on friction and wear properties of n-AT40/Ni-based alloy composite coatings

The effects of speed on the tribological behavior of n-AT40/Ni-based alloy composite coating are shown in Fig. 9. It shows that the friction coefficient of the composite coating is only 0.303 at the speed of 0.21 m/s, which increases to 0.383 as the speed increases to 0.28 m/s, but when the speed is higher than 0.28 m/s, the friction coefficient keeps a steady stage of 0.383–0.391 as shown in Fig. 9(a). The wear loss of the composite coating increases from 1.55 mg to 3.22 mg with the increase of speed (Fig. 9(b)). The average friction coefficient and wear loss of the composite coating are reduced by 13.8% and 36.5%, respectively, compared with the Ni-based alloy coating.

It is obvious that speed has significant influence on the friction and wear properties of the composite coatings. In dry friction condition, most of the friction energy turns into heat energy of the contact surfaces, which results in temperature rising in local contact area to change the strength, hardness and elastic module of the composite coating, furthermore, affects its tribological behavior. The local temperature can be expressed by contact temperature ( $T$ ) and its theoretical calculating formula as follows [25]:

$$T = T_0 + A_1 \frac{\gamma \mu_v \sigma_m V_r}{\sqrt{k \rho c}} \sqrt{t} \quad (10)$$

where  $T_0$  is the environment temperature;  $A_1$  is the circular contact coefficient of 1.11;  $\mu_v$  is the friction coefficient at different speeds;  $\gamma$  is the heat distribution coefficient of 0.45;  $\sigma_m$  is the average contact stress;  $V_r$  is the sliding speed;  $k$  is the thermal conductivity of the composite coating;  $\rho$  is the density of the composite coating;  $c$  is the specific heat capacity of the composite coating at normal pressure;  $t$  is the contact time.

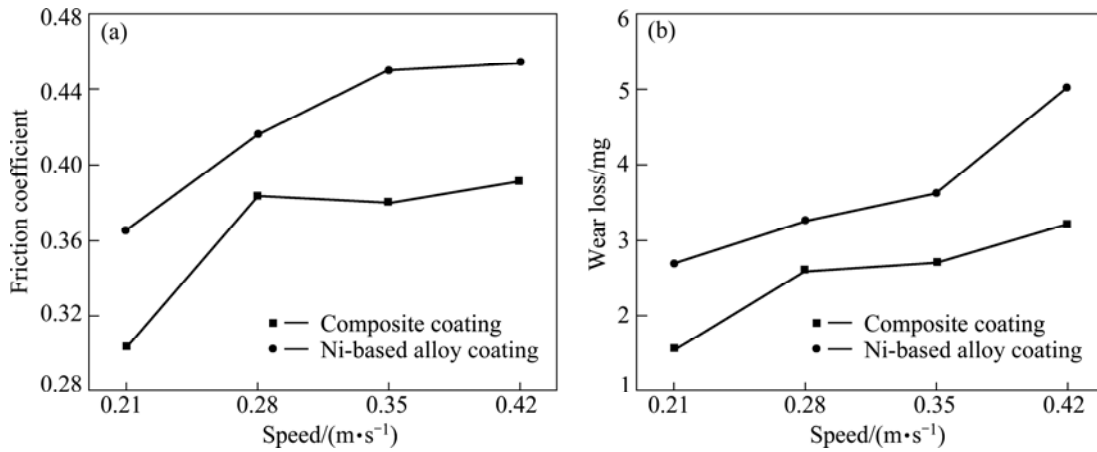
Table 2 lists the contact temperatures of the worn surface at different speeds.

**Table 2** Contact temperatures of worn surfaces at different speeds

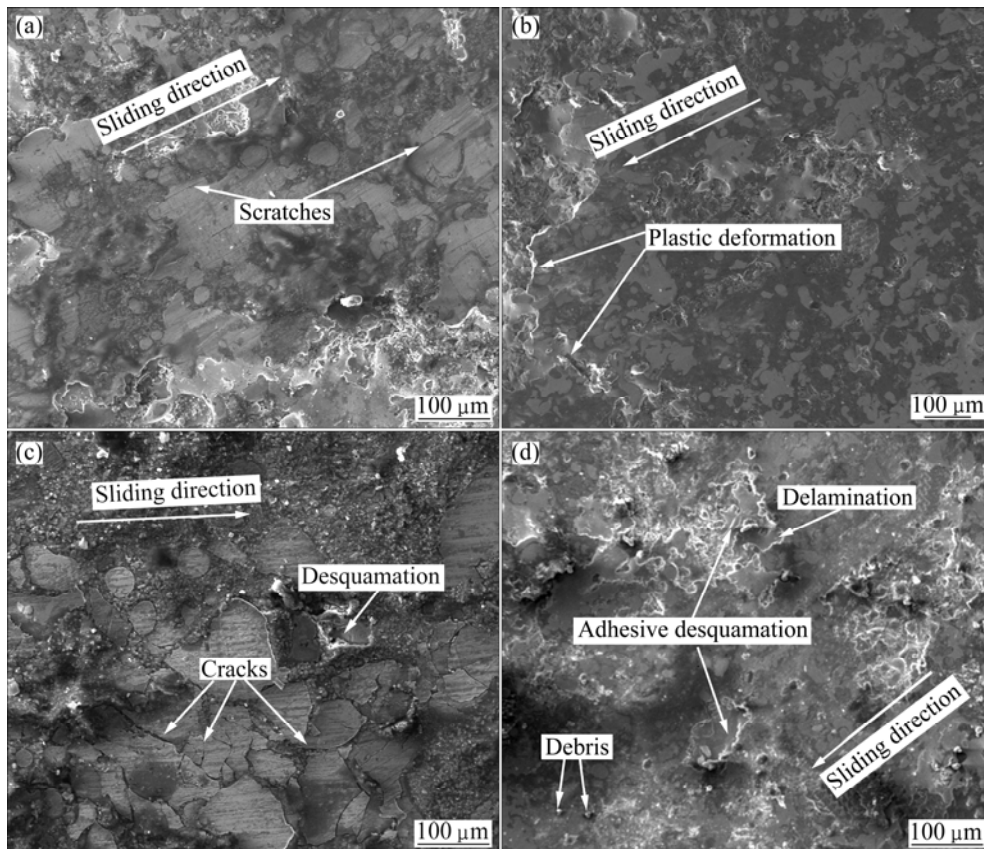
Sliding velocity/(m·s <sup>-1</sup> )	0.21	0.28	0.35	0.42
Contact temperature/°C	519.65	673.41	767.88	850.95

Figure 10 shows the typical worn surface morphologies of the composite coating at different speeds. At the low speed of 0.21 m/s, the contact temperature of the worn surface is 519.65 °C, which hardly affects the mechanical properties of coating

material, so only slight scratches appear on the worn surface as shown in Fig. 10(a). As the speed increases to 0.28 m/s, the contact temperature reaches 673.41 °C and the strength and hardness of the composite coating may be reduced. The worn surface suffers from plastic deformation caused by the continuous extruding and rubbing of GCr15 counterpart that results in multi-plastic deformation wear (Fig. 10(b)). When the speed is 0.35 m/s, plenty of microcracks and desquamation emerge on the worn surface as shown in Fig. 10(c). The contact temperature increases to 767.88 °C at 0.35 m/s, leading



**Fig. 9** Friction coefficient (a) and wear loss (b) of composite coatings at different speeds



**Fig. 10** Typical worn surface morphologies of composite coatings at sliding speeds of 0.21 m/s (a), 0.28 m/s (b), 0.35 m/s (c) and 0.42 m/s (d)

to remarkable plastic deformation in contact area. Meanwhile, the acting frequency of contact stress on the worn surface is also increased. Therefore, microcracks are initiated in the maximum shear stress area and drawbacks of the composite coating, then propagate to surface and result in partial fatigue desquamation of coating material by rubbing action of the GCr15 counterpart [26].

At the high speed of 0.42 m/s, the worn surface takes on evident delamination and adhesive desquamation traces as well as some slight wear debris (Fig. 10(d)). In this friction condition, the contact temperature of the worn surface is as high as 850.95 °C. The instantaneous high temperature results in much more obvious decrease in strength and hardness of coating materials. Consequently, the welding-on between frictional surfaces happens in micro contact area, and then is ruptured by shearing action of friction force. After repeating plastic deformation→welding-on→rupturing process, material transfer from the composite coating to the counterpart is generated that induces adhesive desquamation traces. However, partial adhesive layer with low bonding force to the counterpart is avulsed to form slight wear debris. Compared with the Ni-based alloy coating, the n-AT40 reinforcing particles in composite coating are capable of increasing its strength and avoiding serious adhesive wear. Therefore, the n-AT40/Ni-based alloy composite coating possesses lower friction coefficients and wear losses than the Ni-based alloy coating.

## 4 Conclusions

1) The phases of n-AT40/Ni-based alloy composite coating are  $\gamma$ -Ni,  $\alpha$ -Al<sub>2</sub>O<sub>3</sub>,  $\gamma$ -Al<sub>2</sub>O<sub>3</sub>, rutile-TiO<sub>2</sub>, Al<sub>2</sub>TiO<sub>5</sub>, Cr<sub>23</sub>C<sub>6</sub>, AlNi<sub>3</sub> and FeNi<sub>3</sub>. The microhardness of the composite coating is HV<sub>0.5</sub> 624, which is 13.5% higher than that of the composite coating.

2) In different loads conditions, the friction coefficients of the composite coating vary in the range of 0.360–0.394 and its wear losses change in 1.32–4.49 mg, which are lower than those of the Ni-based alloy coatings. The wear mechanism of the composite coating is micro-cutting wear at loads of 3 N. At the load of 6–12 N, the contact stress of the composite coating is higher than its elastic limit stress, and the wear mechanism changes into multi-plastic deformation wear, abrasive wear and micro-brittle fracture wear.

3) With the increase of speeds, the average friction coefficient and wear loss of the composite coatings are decreased by 13.8% and 36.5%, respectively, compared with those of the Ni-based alloy coating. The contact temperature of the worn surface is 519.65 °C at the low speed of 0.21 m/s, and increases to 850.95 °C as the

speed increases to 0.42 m/s. The wear mechanisms are mainly multi-plastic deformation wear, fatigue wear and adhesive wear.

## References

- [1] DEY S K, PERRY T A, ALPAS A T. Micromechanisms of low load wear in an Al–18.5%Si alloy [J]. *Wear*, 2009, 267: 515–524.
- [2] ZHANG B G, CHEN G Q, ZHANG C G, NI J Q. Structure and mechanical properties of aluminum alloy/Ag interlayer/steel non-centered electron beam welded joints [J]. *Transactions of Nonferrous Metals Society of China*, 2011, 21(12): 2592–2596.
- [3] CHEN Gang, HE Yue-hui, SHEN Pei-zhi. Research actualities on materials and processes of engine piston parts and cylinder liner [J]. *Materials Science and Engineering of Powder Metallurgy*, 2009, 14(4): 205–212. (in Chinese)
- [4] QIN Li-bai, SUN Ting-fu, ZHANG Shu-yong, REN Zheng, HU Lian-ka, HUANG Wen-shu, LI Yan, ZHANG Hua, LIU Huan-en. Wear property of high-silicon aluminum alloy cylinder sleeve [J]. *Ordinance Material Science and Engineering*, 2010, 33(6): 69–72. (in Chinese)
- [5] WU Z H, ZHOU W C, LUO F, ZHU D M. Effect of MoSi<sub>2</sub> content on dielectric and mechanical properties of MoSi<sub>2</sub>/Al<sub>2</sub>O<sub>3</sub> composite coatings [J]. *Transactions of Nonferrous Metals Society of China*, 2012, 22(1): 111–116.
- [6] DEJANG N, LIMPICHAIPANIT A, WATCHARAPASORN A, WIROJANUPATUMP S, NIRANATLUMPONG P, JIANSIRISOMBOON S. Fabrication and properties of plasma-sprayed Al<sub>2</sub>O<sub>3</sub>/ZrO<sub>2</sub> composite coatings [J]. *Journal of Thermal Spray Technology*, 2011, 20(6): 1259–1269.
- [7] ZHU Jing-lei, HUANG Ji-hua, WANG Hai-tao, XU Jun-long, ZHAO Xing-ke, ZHANG Hua. Microstructures of TiC/Fe–Ni metal ceramic composite coatings by reactive plasma spray [J]. *The Chinese Journal of Nonferrous Metals*, 2008, 18(1): 36–41. (in Chinese)
- [8] ALTUNPAK Y, AKBULUT H, USTEL F. The effect of plasma spraying on the microstructure and aging kinetics of the Al–Si matrix alloy and Al–Si/SiC composites [J]. *Journal of Materials Engineering and Performance*, 2010, 19(1): 116–123.
- [9] CHEN Hai-tao, LI Zhong-sheng, SUN Cai-yun, HE Qing-bing, WU Hu-lin. Study on Al<sub>2</sub>O<sub>3</sub>/Ni–Cr–Cr<sub>3</sub>C<sub>2</sub> wearing composite coating and its tribological properties [J]. *Rare Metal Materials and Engineering*, 2011, 40(sp2): 447–451. (in Chinese)
- [10] RICO A, RODRIGUEZ J, OTERO E, ZENG P, RAINFORTH W M. Wear behaviour of nanostructured alumina–titania coatings deposited by atmospheric plasma spray [J]. *Wear*, 2009, 267: 1191–1197.
- [11] LU Lin, MA Zhuang, WANG Fu-chi, LIU Yan-bo. Friction and wear induced of nano and microscale structured Al<sub>2</sub>O<sub>3</sub>–TiO<sub>2</sub> coatings [J]. *Transactions of Beijing Institute of Technology*, 2010, 30(7): 878–882. (in Chinese)
- [12] BATTEZ A H, VIESCA J L, GONZALEZ R, BLANCO D, ASEDEGBEGA E, OSORIO A. Friction reduction properties of a CuO nano lubricant used as lubricant for a NiCrBSi coating [J]. *Wear*, 2010, 268: 325–328.
- [13] WANG Dong-sheng, TIAN Zong-jun, SHEN Li-da, LIU Zhi-dong, HUANG Yin-hui. Microstructure and formation mechanisms of plasma-sprayed nanostructured composite ceramic coatings [J]. *The Chinese Journal of Nonferrous Metal*, 2009, 19(1): 77–83. (in Chinese)
- [14] TIAN Zong-jun, WANG Dong-sheng, SHEN Li-da, LIU Zhi-dong, HUANG Yin-hui. Study on nanostructured Al<sub>2</sub>O<sub>3</sub>–13TiO<sub>2</sub> ceramic coatings by plasma-spraying [J]. *Rare Metal Materials and Engineering*, 2009, 38(10): 1740–1744. (in Chinese)
- [15] BOBZIN K, LUGSCHEIDER E, MAES M, et al. Grain size

- evaluation of pulsed TiAlN nano composite coatings for cutting tools [J]. *Thin Solid Films*, 2007, 515: 3681–3684.
- [16] GAN G S, ZHANG L, BEI S Y, LU Y, YANG B. Effect of TiB<sub>2</sub> addition on microstructure of spray-formed Si–Al30 composite [J]. *Transactions of Nonferrous Metals Society of China*, 2011, 21(10): 2242–2247.
- [17] LI J L, CHEN R S, KE W. Microstructure and mechanical properties of Mg–Gd–Y–Zr alloy cast by metal mound and lost foam casting [J]. *Transactions of Nonferrous Metals Society of China*, 2011, 21(4): 761–766.
- [18] BHUSHAN B. Introduction to tribology [M]. GE Shi-rong. Beijing: China Machine Press, 2006: 59–67. (in Chinese)
- [19] JOHNSON K L. Contact mechanics [M]. Cambridge: Cambridge University Press, 1985: 96–108.
- [20] POPOV V L. Contact mechanics and friction physical principles and applications [M]. LI Qiang, LUO Jian-bin. Beijing: Tsinghua University Press, 2011: 44–48. (in Chinese)
- [21] THIMMARAYAN R, THANIGAIYARASU G. Effect of particle size, forming and ageing on the mechanical fatigue characteristics of Al6082/SiCp metal matrix composites [J]. *International Journal of Advanced Manufacture Technology*, 2010, 48: 625–632.
- [22] WEON P T. Toughness and hardness of hot-pressed TiB<sub>2</sub>–TaB<sub>2</sub> and Ti(C,N)–ZrO<sub>2</sub>–TiB<sub>2</sub> composites at elevated temperature [J]. *Journal of Materials Science Letters*, 2003, 22: 191–193.
- [23] ZHOU Hong-ming, YI Dan-qing, LIU Gong-qi, XIAO Lai-rong. Strengthening and toughening effect and its mechanism for Si<sub>3</sub>N<sub>4</sub>(p)/SiC(w)–MoSi<sub>2</sub> composite[J]. *Rare Metal Materials and Engineering*, 2009, 38(11): 1955–1959. (in Chinese)
- [24] HE L, TAN Y F, CAI B, TAN H, GAO L. Research on friction and wear properties of plasma spraying Ni-base alloy coatings on aluminum alloy surfaces [J]. *Advanced Materials Research*, 2012, 538–541: 207–213.
- [25] LIU Zuo-min. Tribological theory and design [M]. Wuhan: Wuhan University of Technology Press, 2009: 47–55. (in Chinese)
- [26] MAHATO A, XIA S M, PERRY T, SACHDEV A, BISWAS S K. Role of silicon in resisting subsurface plastic deformation in tribology of aluminum-silicon alloys[J]. *Tribology International*, 2010, 43: 381–387.

## 纳米 Al<sub>2</sub>O<sub>3</sub>–40%TiO<sub>2</sub> 复相陶瓷颗粒增强 镍基合金复合涂层的摩擦学性能

何龙, 谭业发, 谭华, 周春华, 高立

解放军理工大学 工程兵工程学院, 南京 210007

**摘要:** 运用等离子喷涂技术在 7005 铝合金表面制备 Al<sub>2</sub>O<sub>3</sub>–40%TiO<sub>2</sub> 纳米结构颗粒增强镍基合金复合涂层, 分析其微观结构, 研究其在不同载荷和速度条件下的摩擦磨损性能。结果表明: 复合涂层主要由  $\gamma$ -Ni、 $\alpha$ -Al<sub>2</sub>O<sub>3</sub>、 $\gamma$ -Al<sub>2</sub>O<sub>3</sub> 和金红石型-TiO<sub>2</sub> 等相组成, 其摩擦因数和磨损失重较镍基合金涂层显著降低。在轻载 3 N 时, 复合涂层磨损表面的接触应力较低, 主要发生微观切削磨损; 当载荷上升至 6~12 N 时, 接触应力高于磨损表面的弹性极限应力, 复合涂层的磨损机理变为多次塑变磨损、微观脆性断裂磨损和磨粒磨损。随着速度的增大, 磨损表面的接触温度逐渐升高, 复合涂层以多次塑变磨损、疲劳磨损和粘着磨损为主。

**关键词:** 纳米 Al<sub>2</sub>O<sub>3</sub>–TiO<sub>2</sub> 复相陶瓷颗粒; 镍基合金; 复合涂层; 等离子喷涂; 摩擦; 磨损

(Edited by Hua YANG)